SPE 39698

Control of Fluid Injection into a Low-Permeability Rock - 1. Hydrofracture Growth

Tad W. Patzek and Dmitriy B. Silin, Department of Materials Science and Mineral Engineering, University of California, Berkeley, Berkeley CA 94720

This paper was prepared for presentation at the 1998 SPE/DOE Improved Oil Recovery Symposium held in Tulsa, Oklahoma, 19–22 April 1998.

Abstract

This paper deals with growth of injection hydrofractures in transient linear flow in a low permeability, soft rock. Seventeen waterflood injectors in Section 12 of the Middle Belridge diatomite, three steam injectors in Section 29 of the South Belridge diatomite, as well as forty four injectors in the Lost Hills I waterflood have been analyzed. The field data show that cumulative injection of water or steam scales with time to the power of 1, rather than ½ predicted from the theory of linear transient flow. In other words, at constant injection pressure, injection rate is remarkably constant. Therefore, either the injection hydrofractures grow with time, or the formation permeability increases with time, or both. A simple mass balance of hydrofracture growth during fluid injection, attributed to Carter, is corrected, extended to the case of variable injection pressure, and presented in a simplified form. The growth of fracture area at constant injection rate is expressed in terms of two easily measured field parameters, the early "injection slope" in linear transient flow, and the average injection rate. Carter's fracture growth rate is further halved to account for the reservoir layer homogeneity parallel and perpendicular to the hydrofracture plane. The Carter theory predictions are then compared with the growth rate of hydrofracture area calculated independently for two steam injectors in Section 29. There is remarkable agreement between the modified Carter theory predictions and the independently estimated rates of growth of these two hydrofractures. We show that fluid injection above a reasonable minimum rate must lead to hydrofracture extension if injection pressure is bounded from above. Ultimately, fracture growth is inevitable, regardless of mechanical design of injection wells and injection policy. We also show that water injection leads to less severe formation damage and fracture extension than steam. By analyzing the thermal and pore stresses, we demonstrate that steam injection may lead to the creation of horizontal fractures, vertical fracture extension, and reservoir damage. Better control of steam injection is, therefore, a must. We address the optimal injection control strategy in Part 2 of this paper.

Introduction

If a "smart" controller of fluid injection into a low permeability reservoir is to recognize a hydrofracture extension, it must either have a built-in model of this process, or it must "learn" the symptoms of several extension events of different magnitudes and intensities. The latter solution would most likely entail using sacrificial injection wells, driven through several pressure steps until their hydrofractures extend catastrophically. Otherwise, the controller would only learn the reservoir and hydrofracture responses to short open-loop tests involving small pressure steps. In such a case, the controller would not be able to generalize from its limited and rather timid experience to catastrophic hydrofracture extensions. The controller's inability to recognize an unknown well behavior would result in a loss of stability and, ultimately, failure. Hence, to design a robust, smart controller, it is important to image and model the *in situ* hydrofracture extensions.

Field demonstrations of hydrofracture propagation and geometry are scarce. Kuo *et al.*[1] proposed a fracture extension mechanism to explain daily wellhead injection pressure behavior observed in the Stomatito Field A fault block in the Talara Area of the Northwest Peru. They have quantified the periodic increases in injection pressure, followed by abrupt decreases, in terms of Carter's theory[2] of hydrofracture extension. Patzek[3] described several examples of injector-producer hydrofracture linkage in the South Belridge diatomite, CA, and quantified the discrete extensions of injection hydrofractures using the linear transient flow theory and linear superposition method.

Vinegar *et al.*[4] used three remote "listening" wells with multiple cemented geophones to triangulate the microseismic events during hydrofracturing of a well in a steam drive pilot in Section 29 of the South Belridge diatomite. Iledero *et al.*[5]

used the same geophone array to triangulate microseismicity during hydrofracturing of two steam injectors nearby. In addition, they corrected the triangulation for azimuthal heterogeneity of the rock by using conical waves. Multiple fractured intervals, each with very different lengths of hydrofracture wings, as well as an unsymmetrical hydrofracture, have been reported.

To date, perhaps the most complete images of hydrofracture shape and growth rate *in situ* have been presented by Kovscek *et al.*[6,7]. They have obtained detailed time-lapse images of two injection hydrofractures in the South Belridge diatomite, Section 29, Phase II steam drive pilot. Using a simplified finite element flow simulator, Kovscek *et al.* calculated the hydrofracture shapes from the time-lapse temperature logs in 7 observation wells. They also used the pilot geology, overall steam injection rates and pressures, and the analysis of Ilderton *et al.*[5] detailing the azimuth and initial extent of the two hydrofractures.

This paper is organized as follows. First, Carter's theory[2] of fracture growth is revisited and extended to the case of variable injection pressure. Carter's assumptions are clarified and corrected. A new, simple expression is obtained for the cumulative fluid injection as a function of variable injection pressure and fracture area. Fracture growth is expressed in terms of readily available field measurements. Second, five field examples of drastic deviations from the linear transient flow theory are shown. These examples involve the time-shifted average of 17 water injectors in the Middle Belridge, three steam injectors in the South Belridge, and 44 water injectors in Lost Hills diatomite. Third, for two steam injectors in the South Belridge diatomite, predictions of the modified[8] Carter theory are compared with the hydrofracture growth calculated independently by Kovscek *et al.*[6,7]. Fourth, the impact of thermal stresses and pore pressure on fracture growth is presented.

Carter's Model Revisited

Let us formulate a one-dimensional model of fluid injection from a vertical highly conductive fracture into a low-permeability rock. We assume to know the entire history of variable injection pressure, the initial fracture area - not necessarily zero, and the entire history of fracture growth. We also assume that the flow of the injected incompressible fluid is horizontal, transient, and perpendicular to the fracture plane. Thus the injection pressure is not communicated beyond the current length of the fracture, and the injection well is in an infinite reservoir. We denote by $A(t)$ and $dA(t)/dt$, respectively, the fracture area and the rate of fracture growth at time t; hence the initial fracture area is $A(0)$. We denote by $q(t)$ and $p_{inj}(t)$ the injection rate and the average downhole injection pressure, respectively. We assume that the permeability inside the fracture is much higher than in the surrounding formation; therefore, at each time the fluid pressure is essentially the same throughout the fracture.

Now let us pick an arbitrary time τ between 0 and t. We define $v_{\tau+\varepsilon\Delta\tau}(t)$, $0<\varepsilon<1$, as the fluid superficial leak-off velocity at time t across that portion of the fracture which opened between τ and $\tau+\Delta\tau$, $\Delta\tau$ being a small increment of time. The new fracture area, which has been created within the time interval $[\tau,\ \tau+\Delta\tau]$, is equal to $A(\tau+\Delta\tau)-A(\tau)$. Hence the rate of fluid leak-off through this area is equal to $\Delta q_\tau(t)=2v_{\tau+\varepsilon\Delta\tau}(t)\big(A(\tau+\Delta\tau)-A(\tau)\big)$. The coefficient of 2 is implied by the assumption that the fracture is two-sided and the fluid leaks symmetrically into the formation. The rate of leak-off from the originally open fracture area is $q_0(t)=2v_0(t)A(0)$. Let us split the time interval $[0,t]$ by a partition $\{0=\tau_0<\tau_1<\ldots<\tau_K=t\}$ into small contiguous nonoverlapping subintervals $[\tau_k,\ \tau_k+\Delta\tau_k]$, $\Delta\tau_k=\tau_{k+1}-\tau_k$ and apply the above calculations to each subinterval. Summing up over all intervals $[\tau_k,\ \tau_k+\Delta\tau_k]$ and adding $wdA(t)/dt$, the rate of water accumulation caused by the fracture extension, one gets:

$$
\begin{aligned}
&q(t)=q_0(t)+\Delta q_0(t)+\Delta q_1(t)+\ldots+\Delta q_{K-1}(t)+w\frac{dA}{dt}=\\
&=2v_0(t)A(0)+2v_{\tau_0+\varepsilon_0\Delta\tau_0}(t)\big(A(\tau_0+\Delta\tau_0)-A(\tau_0)\big)+\\
&+2v_{\tau_1+\varepsilon_1\Delta\tau_1}(t)\big(A(\tau_1+\Delta\tau_1)-A(\tau_1)\big)+\ldots\\
&\ldots+2v_{\tau_{K-1}+\varepsilon_{K-1}\Delta\tau_{K-1}}(t)\big(A(\tau_{K-1}+\Delta\tau_{K-1})-A(\tau_{K-1})\big)+w\frac{dA}{dt}.
\end{aligned}
\tag{1}
$$

Here w is the average fracture width. Passing to the limit as $\max_k(\Delta\tau_k)\to 0$, we obtain

$$
q(t)=2v_0(t)A(0)+2\int_0^t v_\tau(t)\frac{dA(\tau)}{d\tau}\,d\tau+w\frac{dA(t)}{dt}. \tag{2}
$$

Remark. Strictly speaking, the above calculations should yield a single Riemann-Stieltjes integral [9]

$$
2\int_0^t v_\tau(t)\ dA(\tau)
$$

for the first two terms in (2). In this case, $A(t)$ plays the role of a measure defined on $t\ge 0$. Such an integral would automatically incorporate the initial fracture area, $A(0)$, and it would easily handle the case of discontinuous fracture growth. However, one would encounter severe complications from the water sink term $wdA(t)/dt$ in (2), which is proportional to the density of the measure $A(t)$. In order to avoid such difficulties, we assume that $A(t)$ is at least absolutely

continuous on $[0,+\infty)$ and use Eq. (2) with the explicit initial fracture area of $A(0)$. This is a relatively mild restriction because we can always approximate a non-smooth model with a smooth one. Note that the first term in (2) cannot be removed by subtracting $A(0)$ in both time derivatives and dividing through it. Therefore, transforming the fracture area into $\tilde{A}(t) = [A(t) - A(0)]/A(0)$, $\tilde{A}(0) = 0$, does *not* lead to the disappearance of $2v_0(t)$ in (2).

Kuo *et al.*[1], and many others, have essentially expanded Carter's Appendix I in Ref.[2]. Carter, however, *did* assume a zero initial fracture area in his equation (A6). Therefore, the transient mass balance equations, such as Eq. (8.8) and the following in Ref.[10], are in general incorrect and are unjustly attributed to Carter. The mistake of omitting the non-zero initial fracture area and then compensating for it by the physically incorrect "spurt loss," was made at some later time by other authors. We have not attempted to trace the origin of this error.

If the injection pressure is constant, then the leak-off velocity $v_\tau(t)$ depends only on the difference $t-\tau$, i.e., on how long ago from the present the respective portion of the fracture opened. Thus we can substitute $v_\tau(t) = v(t-\tau)$ into (2):

$$q(t) = 2v_0(t)A(0) + 2\int_0^t v(t-\tau)\frac{dA(\tau)}{d\tau}\,d\tau + w\frac{dA(t)}{dt}. \quad (3)$$

Eq. (3) extends the original Carter model[2] of fracture growth by accounting for the initial fracture area $A(0)$.

Now let us find out how $v_\tau(t)$ depends on $p_{inj}(t)$ if the injection pressure varies with time. For this purpose, we consider the following parabolic boundary-value problem on a semi-infinite interval:

$$\begin{aligned}
&\frac{\partial p_\tau}{\partial t} = \alpha\frac{\partial^2 p_\tau}{\partial x^2}, \quad t \ge \tau, \quad x \ge 0,\\
&p_\tau(x,\tau) = \begin{cases} p_{inj}(\tau), & x = 0,\\ p_i, & x > 0,\end{cases}\\
&p_\tau(0,t) = p_{inj}(t).
\end{aligned} \quad (4)$$

Here α and p_i denote, respectively, the constant hydraulic diffusivity and the initial pressure in the formation outside the fracture area created at time τ. The solution to the boundary-value problem (4) characterizes the distribution of pressure outside the fracture caused by fluid injection: $p_\tau(x,t)$ is equal to the pressure at time t at a point located at the distance x from the portion of the fracture, which opened at time τ. According to Darcy's law,

$$v_\tau(t) = -\frac{kk_r}{\mu}\frac{\partial p_\tau(0,t)}{\partial x}. \quad (5)$$

Here k and k_r are the absolute rock permeability and the relative fluid permeability in the formation outside the fracture, and μ is the fluid viscosity.

The solution to the boundary value problem (4) is known (cf. [11], pp. 62-63; or [12], Chapter 3, Section 3):

$$p_\tau(x,t) = p_i + \frac{2}{\sqrt{\pi}}\int_{\frac{x}{2\sqrt{\alpha(t-\tau)}}}^{\infty}\left[p_{inj}\left(t - \frac{x^2}{4\alpha\xi^2}\right) - p_i\right]e^{-\xi^2}\,d\xi, \quad t \ge \tau, \quad x \ge 0, \quad (6)$$

In Appendix A, Eq. (A.4), we prove that

$$\left.\frac{\partial p_\tau(x,t)}{\partial x}\right|_{x=+0} = -\left(\frac{1}{\sqrt{\pi\alpha(t-\tau)}}\left[p_{inj}(\tau) - p_i\right] + \frac{1}{\sqrt{\pi\alpha}}\int_\tau^t \frac{p'_{inj}(\xi)}{\sqrt{t-\xi}}d\xi\right). \quad (7)$$

Substitution into (5) yields

$$v_\tau(t) = \frac{kk_r}{\mu}\left(\frac{1}{\sqrt{\pi\alpha(t-\tau)}}\left[p_{inj}(\tau) - p_i\right] + \frac{1}{\sqrt{\pi\alpha}}\int_\tau^t \frac{p'_{inj}(\xi)}{\sqrt{t-\xi}}d\xi\right) \quad (8)$$

Now it only remains to substitute (8) into (3), take into account that $p_{inj}(t) = p_{inj}(0) + \int_0^\tau p'_{inj}(\tau)\,d\tau$, and change the order of iterated integration:

$$\begin{aligned}
q(t) = {} & w\frac{dA(t)}{dt} +\\
& 2\frac{kk_r}{\mu\sqrt{\pi\alpha}}\left(p_{inj}(0) - p_i\right)\left(\frac{A(0)}{\sqrt{t}} + \int_0^t \frac{1}{\sqrt{t-\xi}}\frac{dA(\xi)}{d\xi}d\xi\right) +\\
& 2\frac{kk_r}{\mu\sqrt{\pi\alpha}}\int_0^t p'_{inj}(\tau)\left(\frac{A(\tau)}{\sqrt{t-\tau}} + \int_\tau^t \frac{1}{\sqrt{t-\xi}}\frac{dA(\xi)}{d\xi}d\xi\right)d\tau.
\end{aligned} \quad (9)$$

Eq. (9) is integrated with respect to time and simplified in Appendix B:

$$Q(t) = wA(t) + 2\frac{kk_r}{\mu\sqrt{\pi\alpha}}\int_0^t \frac{\left(p_{inj}(\tau) - p_i\right)A(\tau)}{\sqrt{t-\tau}}\,d\tau, \quad (10)$$

where $Q(t) = \int_0^t q(\tau)d\tau$ is the cumulative injection at time t.

Eq.(10) is the most general model of fluid injection as a function of injection pressure and fracture area, and under the assumptions listed above. To our knowledge, such an equation has not been published elsewhere. It implies the following

special cases:

(1) If there is no fracture growth and injection pressure is constant, i.e., $A(t) \equiv A_0$ and $p_{inj}(t) \equiv p_{inj}$, then

$$Q(t) = wA_0 + 4A_0 \frac{kk_r}{\mu\sqrt{\pi\alpha}}\left(p_{inj} - p_i\right)\sqrt{t}\,. \tag{11}$$

and injection rate must decrease inversely proportionally to the square root of time:

$$q(t) = 2\frac{kk_r}{\mu\sqrt{\pi\alpha}}\left(p_{inj} - p_i\right)\frac{A_0}{\sqrt{t}} \tag{12}$$

The leak-off velocity is

$$v(t) = \frac{q(t)}{2A_0} = \frac{kk_r}{\mu}\frac{\left(p_{inj} - p_i\right)}{\sqrt{\pi\alpha t}} = \frac{C}{\sqrt{t}}, \quad \text{where } C = \frac{kk_r}{\mu}\frac{\left(p_{inj} - p_i\right)}{\sqrt{\pi\alpha}}. \tag{13}$$

The cumulative fluid injection can be expressed through C:

$$Q(t) = wA_0 + 4A_0\frac{kk_r}{\mu}\frac{\left(p_{inj} - p_i\right)}{\sqrt{\pi\alpha}}\sqrt{t} = wA_0 + 4A_0C\sqrt{t} = wA_0 + \left(\text{Early Injection slope}\right)\sqrt{t}, \tag{14}$$

where the "Early Injection Slope" characterizes fluid injection prior to fracture growth and prior to changes in injection pressure. Note that if *v* is in *ft/day*, then *C* is in $ft/\sqrt{day}$, and from (14) it follows that

$$C = \frac{1}{4A_0}\left(1.127\times10^{-3} \times \text{Early injection slope, BCWE} / \sqrt{\text{Day}}\right). \tag{15}$$

Only in this case, one does not need to know the history of fracture growth and injection pressure in order to calculate injection rate. Eq. (12) provides another proof of inevitability of fracture growth. The only way to prevent it at constant injection pressure is to decrease the injection rate according to $1/\sqrt{t}$. This strategy has not worked in the field[3].

(2) If there is no fracture growth, but injection pressure depends on time, then cumulative injection is

$$Q(t) = wA_0 + 2A_0\frac{kk_r}{\mu\sqrt{\pi\alpha}}\int_0^t \frac{\left(p_{inj}(\tau) - p_i\right)}{\sqrt{t-\tau}}d\tau\,, \tag{16}$$

and injection rate is

$$q(t) = 2\frac{kk_r}{\mu\sqrt{\pi\alpha}}\left(p_{inj}(0) - p_i\right)\frac{A(0)}{\sqrt{t}} + 2\frac{kk_r}{\mu\sqrt{\pi\alpha}}A(0)\int_0^t \frac{p'_{inj}(\tau)}{\sqrt{t-\tau}}\,d\tau. \tag{17}$$

If injection pressure is bounded, $p_{inj}(t) \le P_0$, then

$$Q(t) \le wA_0 + 2A_0\frac{kk_r}{\mu\sqrt{\pi\alpha}}\left(P_0 - p_i\right)\sqrt{t}\,, \tag{18}$$

and, consequently, injection rate cannot satisfy $q(t) \ge q_0$ for all t, if q_0 is also positive because otherwise one would have $Q(t) \ge wA_0 + q_0t$ and contradict (18) for all

$$t > 4\frac{A_0^2\left(P_0 - p_i\right)^2}{q_0^2}\frac{k^2k_r^2}{\mu^2\pi\alpha}\,. \tag{19}$$

The right-hand side of (19) estimates the longest elapsed time of fluid injection at a rate greater than or equal to q_0, without fracture extension and without exceeding maximum injection pressure. For the South Belridge diatomite, this injection time is 100-400 days for $q_0 = 50$ BWPD per fracture at a depth of 1000 ft, the downhole injection pressure increasing to the fracture extension stress, and for reasonable values of all other parameters[13,14]. Thus we conclude that fracture growth is inevitable, regardless of mechanical design of injection wells and injection policy. However, better control of injection pressure through improved mechanical design is always helpful.

(3) At constant injection pressure, both the cumulative injection and the injection rate are completely determined by fracture growth:

$$Q(t) = wA(t) + 2\frac{kk_r}{\mu\sqrt{\pi\alpha}}\left(p_{inj} - p_i\right)\int_0^t \frac{A(\tau)}{\sqrt{t-\tau}}d\tau\,, \tag{20}$$

$$q(t) = w\frac{dA(t)}{dt} + 2\frac{kk_r}{\mu\sqrt{\pi\alpha}}\left(p_{inj} - p_i\right)\left(\frac{A(0)}{\sqrt{t}} + \int_0^t \frac{1}{\sqrt{t-\xi}}\frac{dA(\xi)}{d\xi}d\xi\right). \tag{21}$$

This means that if the fracture stops growing at some time, the injection rate will decrease inversely proportionally to the square root of time. Perhaps the most favorable situation would be obtained if the fracture grew slowly and continuously and supported the desired injection rate at constant pressure. However, since the fracture growth is beyond our control, such ideal situation is hardly possible. We will address the issue of injection control subject to the fracture area growth in Part II of this paper.

If the cumulative injection and injection rate are, respectively, equal to

$$Q(t) = wA_0 + 4\frac{kk_r}{\mu\sqrt{\pi\alpha}}\left(p_{inj} - p_i\right)A_0\sqrt{t} + q_0t \tag{22}$$

and

$$q(t) = 2\frac{kk_w}{\mu\sqrt{\pi\alpha}\sqrt{t}}\left(p_{inj} - p_i\right)A_0 + q_0, \quad (23)$$

then the solution to (21) with respect to $A(t)$ is provided by

$$A(t) = A_0 + \frac{q_0 w}{4\pi C^2}\left[e^{\tau_D}\operatorname{erfc}\left(\sqrt{\tau_D}\right) + \frac{2}{\sqrt{\pi}}\sqrt{\tau_D} - 1\right], \quad (24)$$

where

$$\tau_D = \frac{4\pi C^2}{w^2}t = \frac{\pi}{4}\left(\frac{\text{Early Injection Slope}}{\text{Initial Fracture Volume}}\right)^2 t \quad (25)$$

is the dimensionless drainage time of the initial fracture, and wA_0 is the correct spurt loss from the instantaneous creation of fracture at $t = 0$ and filling it with fluid. The formula (23) for the injection rate consists of two parts: the first component is the leak-off rate when there is no fracture extension and the second, constant, component is "spent" on fracture growth. Conversely, the first constant term in the solution (24) is produced by the first term in (23) and the second additive term is produced by the constant component q_0 of $q(t)$ in (23).

For longer injection times $q(t) \approx q_0$, and it can be shown that

$$A(t) \approx A_0\left(1 + \frac{q_0}{\pi C A_0}\sqrt{t}\right) = A_0\left(1 + \frac{4q_0}{\pi\ \text{Early Injection Slope}}\sqrt{t}\right), \quad (26)$$

where the average fluid injection rate q_0 and the *Early Injection Slope* are in consistent units. For short injection times, the hydrofracture area grows linearly with time (e.g., [10], page 174).

Eq. (26) allows one to calculate the fracture area as a function of average injection rate and the early slope of cumulative injection versus the square root of time. All of these parameters are readily available if one operates a new injection well at a low and constant injection pressure to prevent fracture extension. The initial fracture area (i.e., its length and height) is known approximately from the design of the hydrofracturing job[15,16].

The most important restriction in Carter's and our derivation is the requirement that the injection pressure is not communicated beyond the current length of the fracture. Hagoort *et al*. have shown numerically[8] that for a homogeneous reservoir the fracture propagation rate is only about half of that predicted by the Carter formula (3). This is because the formation pressure increases beyond the current length of the hydrofracture, thus confining it. If fracture growth is slower than predicted by the mass balance (26), then there must be flow parallel[8] to the fracture plane or additional formation fracturing perpendicular to the fracture plane, or both. Either way, the leak-off rate from the fracture must increase.

Injection Fractures Extend. **Fig. 1** demonstrates that the plot of the cumulative water injection versus the square root of time on injection deviates from a straight line for the time-shifted, average injector in the Middle Belridge diatomite. The deviation is positive, and the measured constant water injection rate, **Fig. 2**, exceeds that predicted from the theory of transient linear flow of water, Eq. (23). Similarly, the plots of cumulative steam injected in three injectors in the South Belridge diatomite deviate from straight lines defined by the early injection slopes, **Figs. 3-5**. Instead, the latter three wells inject at constant rates when the injection pressure is constant, **Figs. 6-9**. From these observations, one concludes that either the hydrofracture area grows with time, or the formation permeability increases with time, or both.

Fig. 10 plots Eq. (26) with the parameters from Figs. 1-9 over a period of roughly 7 years. The predicted hydrofracture extensions vary from a factor of 5 for the average waterflood injector in Section 12 to a factor of 7-11 for the three steam injectors in Section 29. Of course, IN2U and IN2L injected for only 4 years, so they never experienced such large fracture extensions. **Fig. 11** shows the same data but with 1/2 of the factor in front of the square root of time in Eq. (26) to account for the reservoir homogeneity perpendicular and parallel to the hydrofracture plane. Now the hydrofractures grow only by a factor of 2.5-5.5 after 7 years of injection.

Clearly, Figs. 10 and 11 predict very large fracture extensions, and these predictions must be verified by an independent experiment. Luckily, an independent interpretation of hydrofracture geometry in the Phase II steam drive pilot[6,7] provides the necessary verification. The latter interpretation relied on lumping the parameters that describe the first-order physics of steam flow in diatomite into a single parameter, called the hydraulic diffusivity. This lumping leads to a second-order partial differential equation, similar in form to a transient diffusion equation, that describes the pressure profile in the steam-occupied zone in each diatomite layer. The method of Marx and Langenheim[17] was then used to locate the steam front in each layer. Finally the transient heat conduction equation was solved for the temperature in the oil zone ahead of the steam front. The hydraulic and thermal diffusivities as well as hydrofracture shape were iterated to match the areal temperature response in each layer of the South Belridge diatomite in the Phase II pilot and the overall cumulative steam injection. The hydrofracture shapes obtained from that analysis are shown in **Figs. 12-13**. There are several fracture extensions lumped into discrete events. In other words, each hydrofracture shape is assumed to persist over a period of time listed below it. In reality, the hydrofracture extensions occur continuously for most of the time, with the exception of, say, a discontinuous change between 225 and 500 days in Fig. 13. The hydrofracture shapes in Figs 12-13 have been integrated, and the corresponding surface areas are plotted in **Figs. 14-15** versus the square root of time, together

with the predictions from Carter's theory modified for the homogeneous reservoir. Agreement between the theory and field data is remarkable.

Fig. 16 shows the cumulative water injection per foot of perforated intervals in 44 wells in the Mobil Lost Hills I waterflood in the diatomite. When plotted versus time, these specific cumulative injection curves are quite close to straight lines indicating gradual fracture extension in almost all wells most of the time. One glaring exception is the most prolific water injector in the entire project, which initially follows the square-root-of time curve, with no fracture extension, with a spectacular fracture failure at 860 days on injection. This well is near a major fault and has injected three times more water than the next three highest injectors, and nine times more than most other injectors. **Fig. 17** is a blow-up of Fig. 16. It shows in more detail that most other slope changes in the specific cumulative injection curves versus time are less dramatic, but also positive. Some of these changes are caused by increases of injection pressure or by acceleration of fracture failure, or both. This behavior is illustrated in more detail in Figs. 11-18 in Ref.[18]. Again, we conclude that fracture extension is a rule, not an exception.

Why Do Injection Fractures Extend?

Thermal stress in a homogeneous, isotropic, and elastic rock is proportional to

$$\Delta\sigma_T = \frac{E\beta\Delta T}{1-\nu}, \tag{27}$$

where E is the Young's modulus, β is the thermal expansion coefficient, ν is Poisson's ratio, and $\Delta T = T - T_{init}$ is temperature increase over the initial rock temperature. If ΔT is negative, as during rock cooling by injected water, the thermal stress is negative, or tensile. Conversely, if ΔT is positive as during rock heating by injected steam, this stress is positive or compressive.

Suppose now that a region of cooled or heated rock, which surrounds a tall vertical hydrofracture, can be described as a vertical cylinder of elliptical cross-section[19,20]. Then the interior thermoelastic stresses parallel to the minimum horizontal in-situ stress, σ_h, and to the maximum horizontal stress, σ_H, are modified, respectively, by two functions of the aspect ratio of the cylinder length, a_{0T}, and width, b_{0T}:

$$\begin{aligned}\Delta\sigma_{hT} &= \frac{E\beta\Delta T}{1-\nu}\frac{b_{0T}/a_{0T}}{1+b_{0T}/a_{0T}},\\ \Delta\sigma_{HT} &= \frac{E\beta\Delta T}{1-\nu}\frac{1}{1+b_{0T}/a_{0T}}.\end{aligned} \tag{28}$$

The subscript T refers to the heated/cooled region of the reservoir. As one can see from Eqs. (28) above, the interior stress parallel to σ_h is changed less than the one parallel to σ_H for narrow long elliptical regions, generated by long injection fractures.

Pore pressure also influences stress in the rock. Lubinski[21] has shown that under the assumption of pressure-independent rock porosity and permeability, the changes of stress $\Delta\sigma_{hP}$ and $\Delta\sigma_{HP}$ induced by a pore pressure change can be computed just like thermal stress

$$\begin{aligned}\Delta\sigma_{hP} &= \frac{EJ\Delta p}{1-\nu}\frac{b_{0P}/a_{0P}}{1+b_{0P}/a_{0P}},\\ \Delta\sigma_{HP} &= \frac{EJ\Delta p}{1-\nu}\frac{1}{1+b_{0P}/a_{0P}},\\ J &\equiv \frac{1-2\nu}{E} - \frac{c_{gr}}{3}.\end{aligned} \tag{29}$$

The subscript P refers to the pressurized or depleted region of reservoir. For simplicity, we assume that the pressured up and cooled/heated rock regions coincide. For hydrofracture dimensions of field magnitude, fracture mechanics studies have shown that the hydrofracture extends when

$$\begin{aligned}p_{inj} &= \sigma_1 + \Delta p_{overpressure},\\ \sigma_1 &= \sigma_h + \Delta\sigma_{hT} + \Delta\sigma_{hP}.\end{aligned} \tag{30}$$

where p_{inj} is the mean injection pressure in the hydrofracture, $\Delta p_{overpressure}$ is the overpressure required to extend the field-scale hydrofracture, and σ_1 is the total stress opposing injection. $\Delta p_{overpressure}$ can be measured[15] or calculated[16]. For example, in the South Belridge diatomite the overpressure is ~100 psi. The total stress opposing injection, σ_1, is the sum of the minimum in-situ stress, and the stresses caused by changes of the rock temperature and the pore pressure. Note that during injection of cooler water, the tensile thermal stress tends to cancel the compressive pore pressure stress. In case of steam, these two stresses add up, and it is *always* more difficult to inject steam than water.

Fracture extension in water injection

Fig. 18 illustrates problems with water injection into the diatomite. The layered rock properties are taken from de Rouffignac[22]. His layer depths are shifted down to correspond with the steam injection well IN2U. Steps in the stress curves in Fig. 18 result from the discontinuous average mechanical properties of the diatomite layers. The rock cooling is set to $\Delta T = -30^0\,F$ and the pore pressuring to $\Delta P = 200$ psi. The pressurized and cooled reservoir zone is assumed to be circular. The downhole water injection pressure may vary. Its maximum is obtained by adjusting the wellhead pressure (WHP) so that the downhole water pressure is equal to the overburden stress at the diatomite top. The minimum WHP is such that the entire hydrofracture stays open. This range of downhole water injection pressures is denoted by ΔP_{inj} in

Fig. 18. Across ΔP_{inj}, the entire hydrofracture will undergo extension, only its top part will extend, or no extension will occur. It is up to the operator to adjust the injection pressure so that it barely exceeds the lowest constraint of $\sigma_h + \Delta\sigma_{hT} + \Delta\sigma_{hP}$. Unfortunately this constraint changes with time, depending on the size and shape of the pressurized and cooled zone, heat conduction, creation of branched fractures orthogonal to the original hydrofracture, and plugging of the hydrofracture with fines[20]. The usual policy of an operator is to increase the injection pressure sufficiently and inject water at an approximately constant rate. This policy leads inevitably to fracture extension later in the project life (cf. Figs. 1-8 and previous section).

Fracture extension in steam injection

As an example, we use the diatomite steam injector IN2U, whose history is detailed in Figs. 7 and 12. Out of 1360 days on injection shown in Fig. 7, IN2U had 166 days with the wellhead pressures of 700-800 psi, 476 days at 800-900 psi, and 377 days at 900-1000 psi, i.e., 63% of the time the wellhead injection pressure was above 800 psi. **Fig. 19** shows that both the fracture extension stress, $\sigma_h + Overpressure$, and the overburden stress, σ_v, are exceeded by the steam pressure. Thus, were it not for the thermal stress, steam injection in IN2U at the most prevalent wellhead pressure of 900 psi would result in an immediate, lengthwise, extension of the vertical fracture up to the top of the injection interval and in creation of a horizontal fracture above it. Strong thermal stresses prevent this from happening for some time. As these stresses relax, fracture extension by steam becomes inevitable. **Fig. 20** shows the thermal and pore pressure stresses resulting from heating and pressuring the rock around IN2U by 150^0F and 200 psi, respectively. Over the injection pressure range of 800-1000 psi, the original vertical hydrofracture is extended across the upper half of the injection interval, and a horizontal fracture is created just above it. No or little fracture extension occurs across the lower half of the injection interval. Both phenomena have been well documented in IN2U[7] and are shown in Fig. 12. Creation of horizontal fractures during hydrofracturing at high pressures is well documented[23] in the top part of the South Belridge diatomite. These fractures occur at the layer boundaries and are caused by the discontinuities of mechanical properties of the rock.

As heating continues, $\Delta T = 180^0 F$, the thermal stresses increase, and prevent further extension of the vertical hydrofracture. However, the horizontal fracture created earlier continues to extend. As a matter of fact, once a horizontal fracture has been created, an increase of σ_1 in Eq. (30) above the overburden stress is irrelevant. The following dilemma becomes obvious: to keep the lower portion of the hydrofracture open, the operator creates a horizontal fracture above it. To close the horizontal fracture, the injection pressure must now decrease to below 900 psi. Once this happens, the lower half of the vertical hydrofracture shuts down, and the injection rate more than halves. This occurs in Fig. 7 after 1000 days on injection. Such a process is self-regulating. When the rock cools down by heat conduction, the injection resumes. With time, the strong thermal stresses, which prevent fracture extension by increasing the minimum in-situ stress, relax. This is caused by heat conduction and convection. Also, in three dimensions, the thermal stress relaxes by diffusing the local volumetric rock expansion all the way up to the surface, which is subject to zero total stress. In other words, the rock rearranges, and the extra stresses fade away. At this point, steam injection is *no* longer feasible, and it will inevitably result in reservoir damage. On the other hand, if steam injection causes the rock to consolidate and strengthen mechanically, then higher injection pressures become feasible with time. Indeed at high steam temperatures and pressures, amorphous diatomite may undergo diagenetic transformation to a denser and more competent Opal CT. The increase of rock density is equivalent to cooling it down and imposing a tensile stress. This may result in fractures orthogonal to the hydrofracture plane and may cause an increase of rock permeability in the transition zone from Opal A to Opal CT.

Conclusions

1. We have corrected Carter's transient mass balance of fluid injection through a growing fracture and extended it to the case of variable injection pressure.
2. We have integrated the extended Carter formula with respect to time and presented it in a new simplified form.
3. We have proved that rate of fluid injection through a fracture cannot be kept above a set positive value indefinitely if injection pressure is bounded from above and the fracture does not grow. In practice, the injection rate must go to zero without fracture growth.
4. Thus, ultimately, fracture growth is inevitable, regardless of mechanical design of injection wells and injection policy. However, better control of injection pressure through improved mechanical design is always helpful.
5. In diatomite, fracture extension must occur no later than 100-400 days for water injection rates of no less than 50 BPD per fracture and downhole injection pressure increasing up to the fracture extension stress.
6. In 20 fluid injection wells in three different locations in the Belridge diatomite and some 40 water injectors in Lost Hills, the respective hydrofractures underwent continuous extension with occasional, discrete failures. Therefore, as we have predicted, extensions of injection hydrofractures are a norm in the low permeability diatomite.
7. These hydrofracture extensions manifested themselves as constant injection rates at constant injection pressures.
8. The magnitude of hydrofracture extension can be predicted over a 4-7 year time period from the initial slope of cumulative injection versus the square root of time, average injection rate, and by assuming a homogeneous reservoir.
9. The hydrofracture areas may extend by a factor of 2.5-5.5 after 7 years of water or steam injection.

10. For two steam injectors in the South Belridge diatomite, the hydrofracture growth predictions from the modified Carter theory were found in excellent agreement with their growth rates calculated independently by Kovscek *et al*.[6,7]
11. We have calculated the thermal and pore pressure stresses in the diatomite and shown that for downhole water injection pressures used in the field, the entire hydrofracture may undergo extension, only its top part may extend, or no extension occurs. Water injection may also lead to fracture branching.
12. Injection of steam into the diatomite is likely to cause more severe problems than injection of water.
13. We have shown that without the thermal stresses, steam injection in the shallow well in S. Belridge Section 29 would result in an immediate extension of the vertical fracture up to the top of the injection interval and in creation of a horizontal fracture above it. Strong thermal stresses prevent this from happening for some time.
14. As the thermal stresses relax, fracture extension and reservoir damage by steam becomes inevitable.
15. Careful control of steam injection is a must, not a luxury.

Nomenclature

A = fracture area, ft^2
w = fracture width, ft
q = injection rate, Bbl/Day
p_{inj} = injection pressure, psi
v = fluid superficial leak-off velocity, ft/Day
α = hydraulic diffusivity, ft^2/Day
p_i = initial pressure in the formation outside the fracture, psi
k = absolute rock permeability, md
k_r = relative permeability to the fluid
μ = the fluid viscosity, cp
E = Young's modulus, psi
ν = Poisson's ratio
c_{gr} = compressibility of rock grains, 1/psi

Acknowledgements

This work was supported in part by two members of the U.C. Oil® Consortium, Chevron Petroleum Technology Company, and CalResources (now Aera Energy), LLC. Partial support was also provided by the Assistant Secretary for Fossil Energy, Office of Gas and Petroleum Technology, under contract No. DE-ACO3-76FS00098 to the Lawrence Berkeley National Laboratory of the University of California. We thank CalResources for releasing the Phase II steam pilot data, and Crutcher-Tufts for releasing the Dow-Chanslor waterflood data. We also thank Mobil E&P US for providing the Lost Hills I waterflood data.

References

1. M. C. T. Kuo, Hanson, H. G., and DesBrisay, C. L., in *Paper SPE 12769, Prediction of Fracture Extension During Waterflood*, Long Beach, 1984 (SPE), p. 377-385.
2. R. D. Carter, Drill. and Prod. Prac., API**,** 261-268 (1957).
3. T. W. Patzek, in Paper SPE 24040, Surveillance of South Belridge Diatomite, Bakersfield, 1992 (SPE).
4. H. J. Vinegar, et al., JPT **44,** 28 (1992).
5. D. Ilderton, Patzek, T. E., Rector, J. W., and Vinegar, H. J., SPE Formation Evaluation**,** 46-54 (1996).
6. A. R. Kovscek, Johnston, R. M., and Patzek, T.W., In Situ **20,** 289-309 (1996).
7. A. R. Kovscek, Johnston, R. M., and Patzek, T.W., In Situ **20,** 251-289 (1996).
8. J. Hagoort, Weatherill, B. D., and Settari, A., SPEJ**,** 293-303 (1980).
9. I. P. Natanson, *Theory of functions of a real variable* (Ungar Pub. Co., New York, 1955).
10. P. Valko, and Economides, M. J., *Hydraulic Fracture Mechanics* (John Wiley & Sons, Inc., New York, 1995).
11. J. C. Carslaw, and Jaeger, J. C., *Conduction of Heat in Solids*, 2 ed. (Clarendon Press, Oxford, 1959).
12. A. N. Tikhonov, and Samarskii, A. A., *Equations of mathematical physics* (Macmillan, New York, 1963).
13. E. D. Zwahlen, and Patzek, T. W., in SPE 38290, Linear Transient Flow Solution for Primary Oil Recovery with Infill and Conversion to Water Injection, Long Beach, 1997 (SPE).
14. E. D. Zwahlen, and Patzek, T. W., In Situ **21,** 297-331 (1997).
15. J. Shlapobersky, Walhaug, W. W., Sheffield, R. E., and Huckabee, P. T., in SPE 18195, Field Determination of Fracturing Parameters for Overpressure Calibrated Design of Hydraulic Fracturing, Houston, TX, 1988 (SPE).
16. J. Shlapobersky, Walhaug, W. W., in SPE 18194, Overpressure Calibrated Design of Hydraulic Fracture Stimulations, Houston, TX, 1988 (SPE).
17. J. W. Marx, and Langenheim, R. H., Trans. AIME **216,** 312-215 (1959).
18. M. Nikravesh, Kovscek, A. R., Murer, A. S., and Patzek, T. W., in SPE 35271, Neural Networks for Field-Wise Waterflood Management in Low Permeability, Fractured Oil Reservoirs, Anchorage, AL, 1996.
19. R. D. Mindlin, and Cooper, H. L., J. Applied Mechanics **Sept.,** 265-68 (1950).
20. T. K. Perkins, and Gonzalez, J. A., SPEJ **25,** 78-88 (1985).
21. A. Lubinski, Proc. Second U.S. Natl. Cong. Appl. Mech.**,** 247 (1954).
22. E. de Rouffignac, and Cherubini, E. E., in *Diatomite Compaction: Experiments and Modeling*, Chevron Oilfield Research Company, La Habra, CA, 1992 (Chevron).
23. C. A. Wright, Davis, E. J., Weijers, L., Minner, W. A., Hennigan, C. M., and Golich, G. M., in *SPE 38324, Horizontal Hydraulic Fractures: Oddball Occurrances or Practical Engineering*, Long Beach, CA, 1997.

Appendix A - Injection pressure gradient for variable injection pressure

Differentiation of Eq. (6) with respect to the distance from the injection fracture yields

$$\frac{\partial p_\tau(x,t)}{\partial x} = -\frac{2}{\sqrt{\pi}}\frac{1}{2\sqrt{\alpha(t-\tau)}}\left[p_{inj}(0) - p_i\right]e^{-\frac{x^2}{4\alpha(t-\tau)}} +$$

$$+\frac{2}{\sqrt{\pi}}\int\limits_{\frac{x}{2\sqrt{\alpha(t-\tau)}}}^{\infty} p'_{inj}\left(t-\frac{x^2}{4\alpha\xi^2}\right)\left(-\frac{2x}{4\alpha\xi^2}\right)e^{-\xi^2}d\xi. \quad (A.1)$$

To calculate the injection rate in (5), we have to pass to the limit as $x \to +0$. First, we define the following expressions:

$$I_1(x) \equiv -\frac{1}{\sqrt{\pi\alpha(t-\tau)}}\left[p_{inj}(0)-p_i\right]e^{-\frac{x^2}{4\alpha(t-\tau)}},$$

$$I_2(x) \equiv \frac{2}{\sqrt{\pi}}\int\limits_{\frac{x}{2\sqrt{\alpha(t-\tau)}}}^{\infty} p'_{inj}\left(t-\frac{x^2}{4\alpha\xi^2}\right)\left(-\frac{2x}{4\alpha\xi^2}\right)e^{-\xi^2}d\xi.$$

Clearly,

$$\lim_{x\to+0} I_1(x) = -\frac{1}{\sqrt{\pi\alpha(t-\tau)}}\left[p_{inj}(0)-p_i\right], \quad t>\tau. \quad (A.2)$$

Let us now calculate $\lim\limits_{x\to+0} I_2(x)$. For this purpose we introduce a new variable $\eta = \dfrac{x}{2\alpha\xi}$. Then

$$I_2(x) = -\frac{2}{\sqrt{\pi}}\int_0^{\sqrt{(t-\tau)/\alpha}} p'_{inj}\left(t-\alpha\eta^2\right)e^{-\frac{x^2}{4\alpha^2\eta^2}}d\eta.$$

Assuming that the function $p'_{inj}(t)$ is bounded and integrable, we can prove that

$$\lim_{x\to+0} I_2(x) = -\frac{2}{\sqrt{\pi}}\int_0^{\sqrt{(t-\tau)/\alpha}} p'_{inj}\left(t-\alpha\eta^2\right)d\eta. \quad (A.3)$$

Indeed, let us choose an arbitrary $\varepsilon > 0$ and select $\delta_1 > 0$ such that

$$\left|\frac{4}{\sqrt{\pi}}\int_0^{\delta_1} p'_{inj}\left(t-\alpha\eta^2\right)d\eta\right| < \frac{\varepsilon}{2}.$$

Then the following chain of estimates holds true:

$$\left|I_2(x)-\left(-\frac{2}{\sqrt{\pi}}\int_0^{\sqrt{(t-\tau)/\alpha}} p'_{inj}\left(t-\alpha\eta^2\right)d\eta\right)\right| \le$$

$$\le \left|\frac{2}{\sqrt{\pi}}\int_0^{\delta_1} p'_{inj}\left(t-\alpha\eta^2\right)\left(1-e^{-\frac{x^2}{4\alpha^2\eta^2}}\right)d\eta\right| +$$

$$\left|\frac{2}{\sqrt{\pi}}\int_{\delta_1}^{\sqrt{(t-\tau)/\alpha}} p'_{inj}\left(t-\alpha\eta^2\right)\left(1-e^{-\frac{x^2}{4\alpha^2\eta^2}}\right)d\eta\right| \le$$

$$\le \left|\frac{4}{\sqrt{\pi}}\int_0^{\delta_1} p'_{inj}\left(t-\alpha\eta^2\right)d\eta\right| +$$

$$\left|\frac{2}{\sqrt{\pi}}\int_{\delta_1}^{\sqrt{(t-\tau)/\alpha}} p'_{inj}\left(t-\alpha\eta^2\right)d\eta\right| \max_{\delta_1\le\eta\le\sqrt{(t-\tau)/\alpha}}\left(1-e^{-\frac{x^2}{4\alpha^2\eta^2}}\right).$$

Notice that

$$\max_{\delta_1\le\eta\le\sqrt{(t-\tau)/\alpha}}\left(1-e^{-\frac{x^2}{4\alpha^2\eta^2}}\right) = 1-e^{-\frac{x^2}{4\alpha^2\delta_1^2}}.$$

Select $\delta > 0$, such that

$$\left(1-e^{-\frac{x^2}{4\alpha^2\delta_1^2}}\right)\left|\frac{4}{\sqrt{\pi}}\int_{\delta_1}^{\sqrt{(t-\tau)/\alpha}} p'_{inj}\left(t-\alpha\eta^2\right)d\eta\right| \le \frac{\varepsilon}{2},$$

whenever $|x| < \delta$. Then, for such an x, one obtains

$$\left|I_2(x)-\left(-\frac{2}{\sqrt{\pi}}\int_0^{\sqrt{(t-\tau)/\alpha}} p'_{inj}\left(t-\alpha\eta^2\right)d\eta\right)\right| \le \varepsilon$$

and the proof is complete.

By adding Eqs. (A.2) and (A.3), and changing the variable of integration $\xi = t-\alpha\eta^2$, we obtain

$$\left.\frac{\partial p_\tau(x,t)}{\partial x}\right|_{x=+0} = -\left(\frac{1}{\sqrt{\pi\alpha(t-\tau)}}\left[p_{inj}(\tau)-p_i\right]+\frac{1}{\sqrt{\pi\alpha}}\int_\tau^t \frac{p'_{inj}(\xi)}{\sqrt{t-\xi}}d\xi\right). \quad (A.4)$$

Appendix B - Derivation of Equation (10)

For a continuously differentiable function $f(t)$ one has

$$\frac{d}{dt}\int_\tau^t \frac{f(\xi)}{\sqrt{t-\xi}}d\xi = \frac{f(\tau)}{\sqrt{t-\tau}}+\int_\tau^t \frac{f'(\xi)}{\sqrt{t-\xi}}d\xi. \quad (B.1)$$

Then the second term in (9) is equal to

$$2\frac{kk_r}{\mu\sqrt{\pi\alpha}}\left(p_{inj}(0)-p_i\right)\frac{d}{dt}\int_0^t\frac{1}{\sqrt{t-\xi}}A(\xi)d\xi\,. \qquad \text{(B.2)}$$

Let us transform the last term in (9). For the function under the integral one obtains

$$\frac{A(\tau)}{\sqrt{t-\tau}}+\int_\tau^t\frac{1}{\sqrt{t-\xi}}\frac{dA(\xi)}{d\xi}d\xi=\frac{d}{dt}\int_\tau^t\frac{1}{\sqrt{t-\xi}}A(\xi)d\xi. \qquad \text{(B.3)}$$

Notice that $p'_{inj}(t)=\frac{d}{dt}\left(p_{inj}(t)-p_i\right)$. Therefore, one has

$$\int_0^t p'_{inj}(\tau)\left(\frac{A(\tau)}{\sqrt{t-\tau}}+\int_\tau^t\frac{1}{\sqrt{t-\xi}}\frac{dA(\xi)}{d\xi}d\xi\right)d\tau=$$

$$\int_0^t\frac{d}{d\tau}\left(p_{inj}(\tau)-p_i\right)\frac{d}{dt}\left(\int_\tau^t\frac{1}{\sqrt{t-\xi}}A(\xi)d\xi\right)d\tau=$$

$$\frac{d}{dt}\left(\int_0^t\frac{d}{d\tau}\left(p_{inj}(\tau)-p_i\right)\int_\tau^t\frac{1}{\sqrt{t-\xi}}A(\xi)d\xi\;d\tau\right)-$$

$$\left(p_{inj}(t)-p_i\right)\int_t\frac{1}{\sqrt{t-\xi}}A(\xi)d\xi=$$

$$\frac{d}{dt}\left(\int_0^t\frac{d}{d\tau}\left(p_{inj}(\tau)-p_i\right)\int_\tau^t\frac{1}{\sqrt{t-\xi}}A(\xi)d\xi\;d\tau\right).$$

We can integrate by parts the expression inside the brackets:

$$\int_0^t\frac{d}{d\tau}\left(p_{inj}(\tau)-p_i\right)\int_\tau^t\frac{1}{\sqrt{t-\xi}}A(\xi)d\xi\;d\tau=$$

$$-\left(p_{inj}(0)-p_i\right)\int_0^t\frac{1}{\sqrt{t-\xi}}A(\xi)d\xi$$

$$+\int_0^t\left(p_{inj}(\tau)-p_i\right)\frac{1}{\sqrt{t-\xi}}A(\xi)\,d\tau.$$

Thus

$$\int_0^t p'_{inj}(\tau)\left(\frac{A(\tau)}{\sqrt{t-\tau}}+\int_\tau^t\frac{1}{\sqrt{t-\xi}}\frac{dA(\xi)}{d\xi}d\xi\right)d\tau=$$

$$\frac{d}{dt}\left(-\left(p_{inj}(0)-p_i\right)\int_0^t\frac{1}{\sqrt{t-\xi}}A(\xi)d\xi\right. \qquad \text{(B.4)}$$

$$\left.+\int_0^t\left(p_{inj}(\tau)-p_i\right)\frac{1}{\sqrt{t-\xi}}A(\xi)\,d\tau\right)$$

Now it remains to substitute (B.2) and (B.4) into (9) in order to obtain

$$q(t)=w\frac{dA(t)}{dt}+2\frac{kk_r}{\mu\sqrt{\pi\alpha}}\frac{d}{dt}\left(\int_0^t\left(p_{inj}(\tau)-p_i\right)\frac{1}{\sqrt{t-\xi}}A(\xi)\,d\tau\right), \qquad \text{(B.5)}$$

which immediately implies (10).

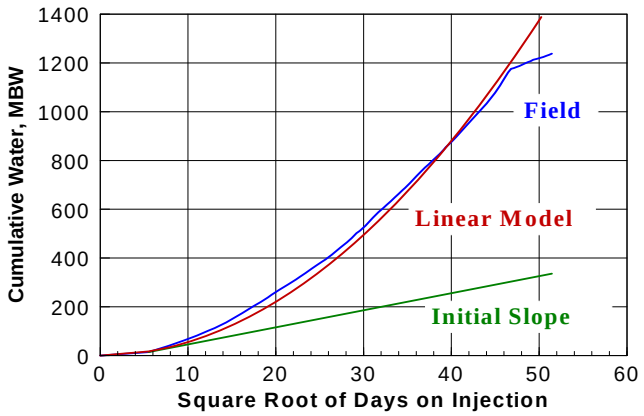

Fig. 1. - Time shifted cumulative water injection per well in Section 12, Dow-Chanslor Fee, Middle Belridge, Crutcher-Tufts. There are 17 injectors. Note a large positive deviation from the initial injection slope of 7000 BW/$\sqrt{\text{Day}}$. A constant injection rate model fits the field data very well over an 8-year period. The average injection rate of water is 550 BW/Day per well.

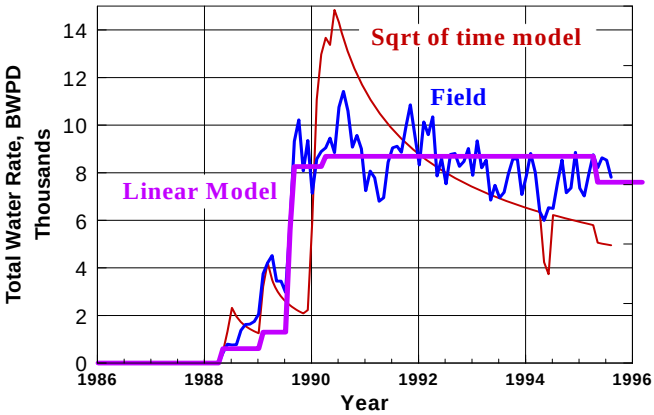

Fig. 2. Total water injection rate in 17 wells in the Crutcher-Tufts waterflood. This rate is almost constant, in contrast to a $1/\sqrt{t}$ decrease required by transient linear flow. Hence the injection hydrofractures must extend. The rate jump in 1989 was caused by new injectors.

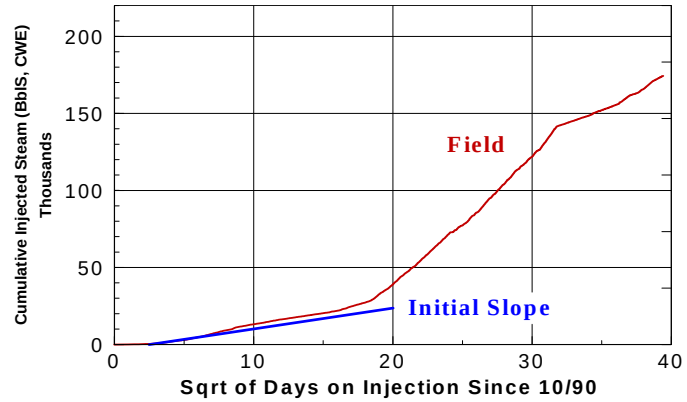

Fig. 3. - Cumulative steam injection in IN2U, Phase II Steam Drive Pilot, Section 29, South Belridge diatomite, CalResources. Note a large positive deviation from the initial injection slope of 1350 BS CWE $\sqrt{\text{Day}}$. Also note two distinct segments of parabolas that follow. The first break in slope is caused by a discrete, large fracture extension and the second one by a decrease of injection pressure.

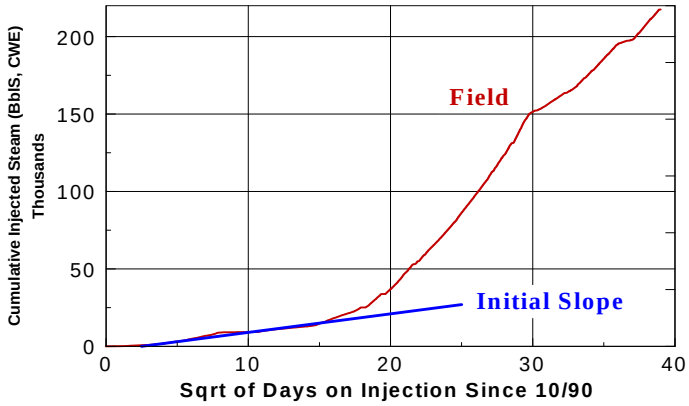

Fig. 4. - Cumulative steam injection in IN2L, Phase II Steam Drive Pilot, Section 29, South Belridge diatomite, CalResources. Note a large positive deviation from the initial injection slope of 1200 BS CWE $\sqrt{\text{Day}}$. The break in slope at 30 $\sqrt{\text{Day}}$ is caused by a decrease of the injection pressure.

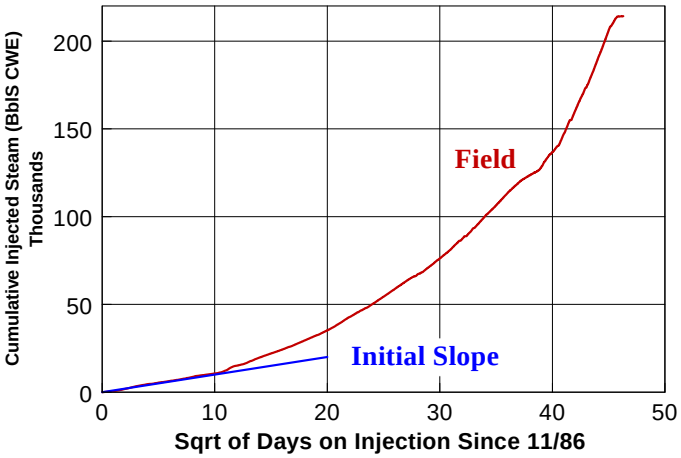

Fig. 5. - Cumulative steam injection in 7IN1, Phase I Steam Drive Pilot, Section 29, South Belridge diatomite, CalResources. Note a large positive deviation from the initial injection slope of 1000 BS CWE $\sqrt{\text{Day}}$.

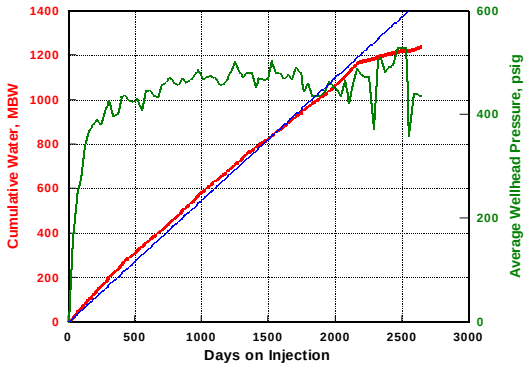

Fig. 6 - Cumulative water injection in an average Section 12 well versus elapsed time on injection. Note that this is a time-shifted average of 17 wells. The shorter elapsed times have contributions from newer, higher injectivity wells, whereas the longest elapsed times are dominated by the old injectors. Hence some initial curvature in the cumulative injection and a definite break at 2100 days. The constant average injection rate of 550 BW/Day defines the fit.

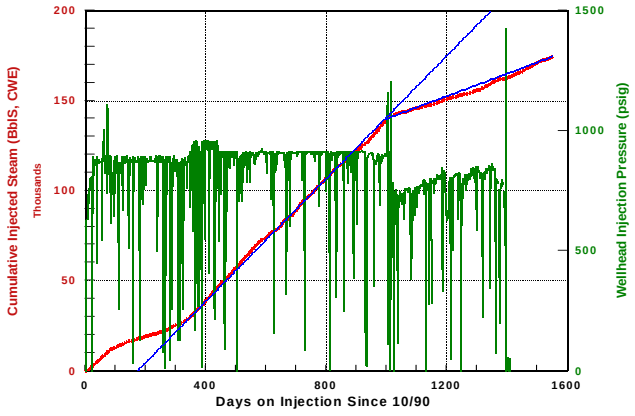

Fig. 7 - Cumulative steam injection in IN2U versus time on injection. Note that between 0 and 1000 days, the injection pressure was relatively constant. At 1000 days, the injection pressure was

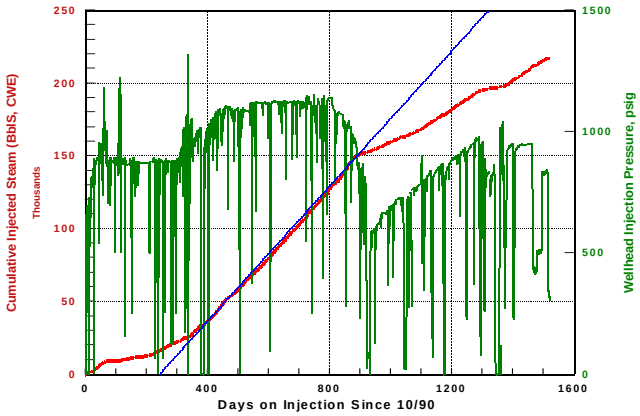

Fig. 8 - Cumulative steam injection in IN2L versus time on injection. Note that between 400 and 800 days, the injection pressure was relatively constant. At 900 days, the injection pressure was decreased

decreased by some 150 psi and then ramped up somewhat over the following 400 days. The constant average injection rate of 170 BS CWE/Day defines the first fit and 63 BS CWE/Day the second one, respectively.

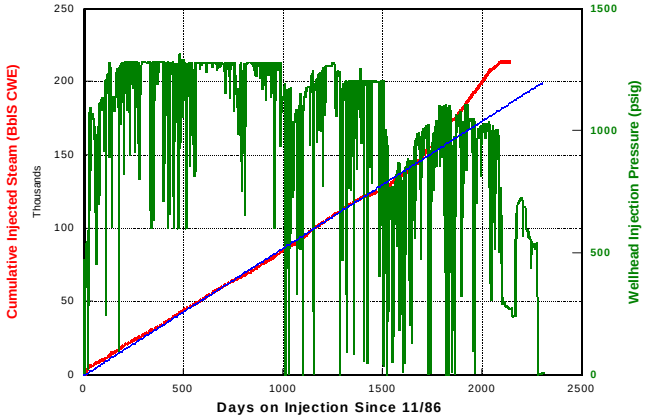

Fig. 9 - Cumulative steam injection in 7IN1 versus time on injection. Note that between 200 and 1500 days the injection pressure was relatively constant. At 1500 days a discrete and large fracture extension occurred with the concomitant drop in injection pressure. The constant average injection rate of 68 BS CWE/Day defines the fit over a 4-year time period.

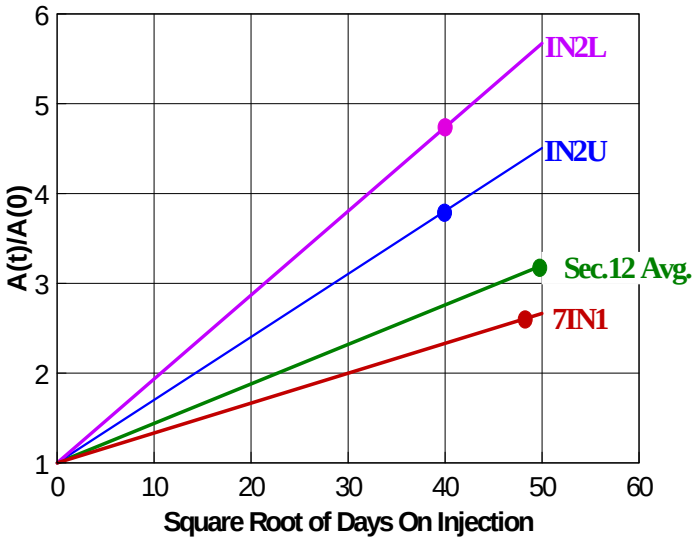

Fig. 11 - Relative extensions of the hydrofracture areas for a homogeneous reservoir. The predictions are 50% of those based on Carter's theory and are in agreement with the simulations by Hagoort *et al*. Note that after 900 days, the hydrofracture in IN2U extends roughly by a factor of 3 and that in IN2L by a factor of 4.

by 300 psi and then ramped up over the following 400 days. The constant average injection rate of 195 BS CWE/Day defines the fit.

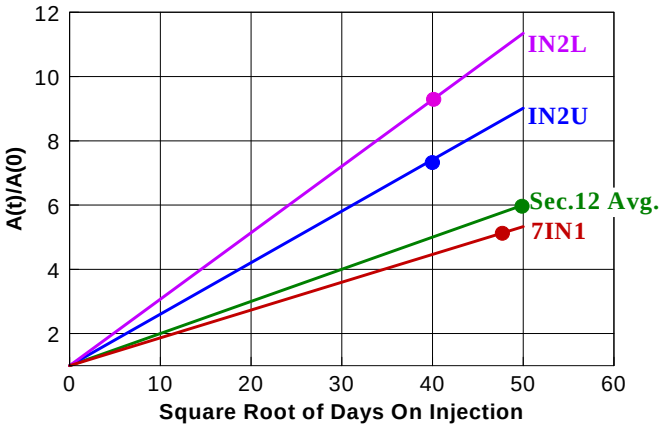

Fig. 10- Relative extensions of the hydrofracture area predicted by Carter's theory of one-dimensional fluid flow perpendicular to the hydrofracture. Note that the average Section 12 waterflood injector underwent roughly half of the hydrofracture extension of IN2L. The dots denote end of field data.

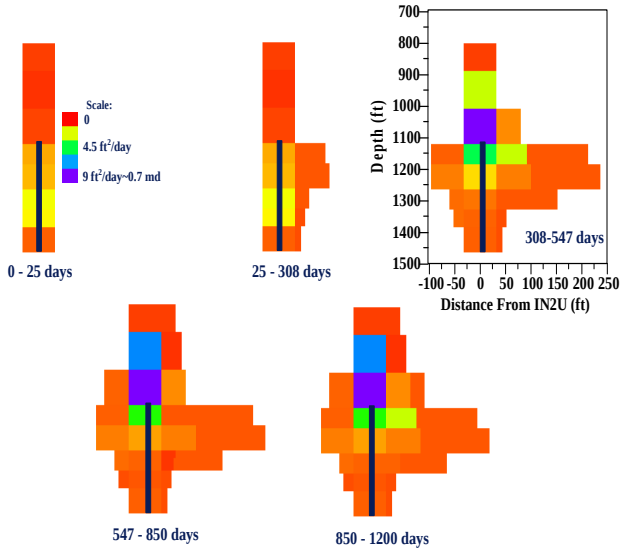

Fig. 12 - Side view of the west face of IN2U hydrofracture and hydraulic diffusivities from history matching. Note that the hydrofracture is highly asymmetric about the injection interval. Also note that the hydraulic diffusivity (formation permeability perpendicular to the hydrofracture) increased significantly with time along relatively few channels. The biggest increase occurred directly above the top of the injection interval and is ascribed to the development of a horizontal fracture (from *In-Situ* 20(3), Figure 3A and 3B, pp. 294-295, 1997).

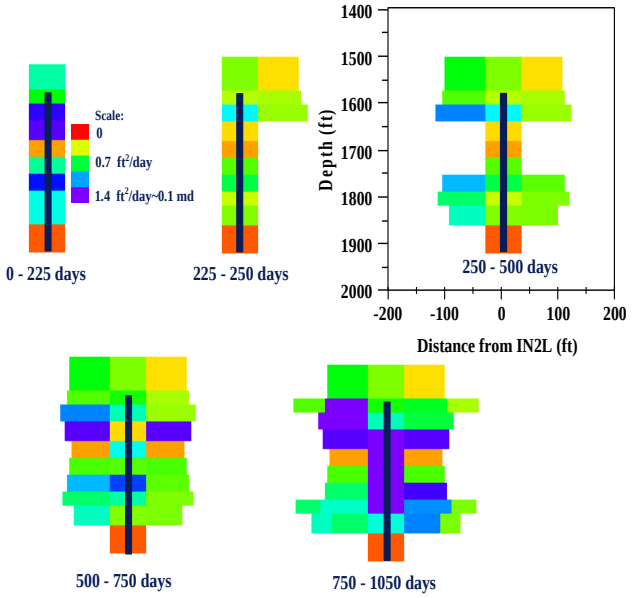

Fig. 13 - Side view of the east face of IN2L hydrofracture and hydraulic diffusivities from history matching. Note that the hydrofracture is symmetric about the injection interval. Also note that the hydraulic diffusivity (formation permeability perpendicular to the hydrofracture) increased significantly with time along numerous channels. These increases were caused by a producer only 40 ft east of the hydrofracture (from *In-Situ* 20(3), 1997).

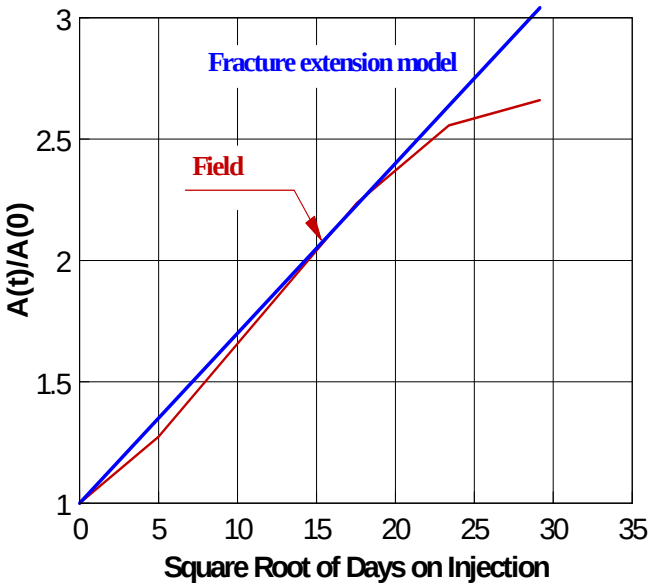

Fig. 14 - Growth of the hydrofracture area in IN2U. The discrete extensions are assumed to have occurred at the beginning of each time interval shown in Fig.12. The homogeneous reservoir prediction agrees very well with the independently obtained hydrofracture areas. Note that at early injection times, the hydrofracture grows linearly with time.

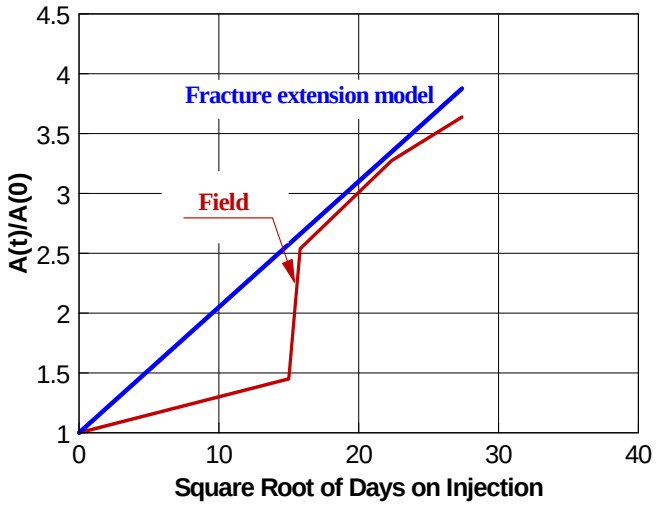

Fig. 15 - Growth of the hydrofracture area in IN2L. The discrete extensions are assumed to have occurred at the beginning of each time interval shown in Fig.13. The homogeneous reservoir prediction agrees very well with the independently obtained hydrofracture areas. The third fracture extension in Fig.13 is catastrophic, and it cannot be predicted by the current model.

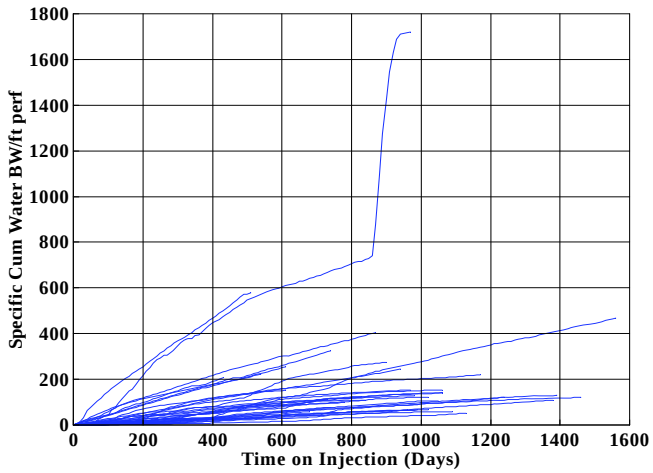

Fig. 16 - Cumulative water injection per foot of perforated intervals versus time in 44 wells in the Mobil Lost Hills I waterflood project. Note that most wells plot close to straight lines, indicating gradual fracture extension. The most prolific injector is an exception. It follows the square-root-of time curve until a catastrophic fracture extension. This injector has injected 3 times more water per unit reservoir thickness than the next two largest injectors and 9 times more than most other wells.

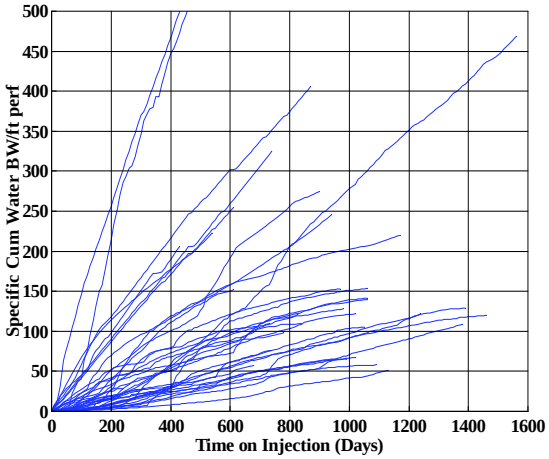

Fig. 17 - A blow up of Fig. 16, showing the cumulative water injection per foot of perforated intervals in 44 wells in the Lost Hills I waterflood. Gradual fracture extension is evident in most of these wells. The increases in slope are caused by increases of injection pressure, or accelerated fracture failure, or both.

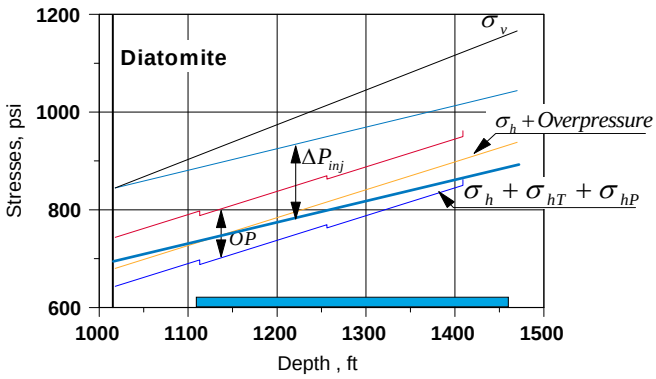

Fig. 18 - Water injection over a pressure range ΔP_{inj} may or may not extend the hydrofracture.

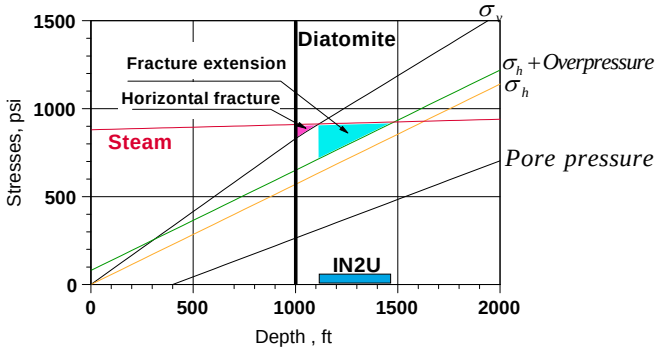

Fig. 19 - Were it not for thermal stresses, steam injection in IN2U at the most prevalent wellhead pressure of 900 psi would result in an immediate fracture extension up to the top of the injection interval and a horizontal fracture above it. Strong thermal stresses prevent this from happening for some time. As these stresses relax, fracture extension becomes inevitable.

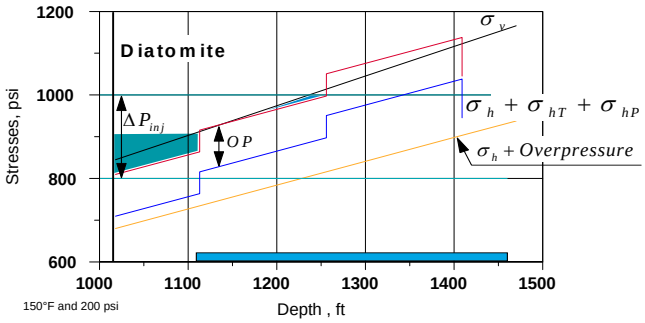

Fig. 20 - Thermal and pore pressure stresses resulting from heating and pressuring the rock around IN2U by 150^{0}F and 200 psi, respectively. Over the injection pressure range of 800-1000 psi, the original vertical hydrofracture is extended over the upper half of the injection interval and a horizontal fracture is created just above it. Both phenomena have been documented in IN2U[7] and are shown in Fig. 12.
extend and no further extension of the vertical hydrofracture occurs.

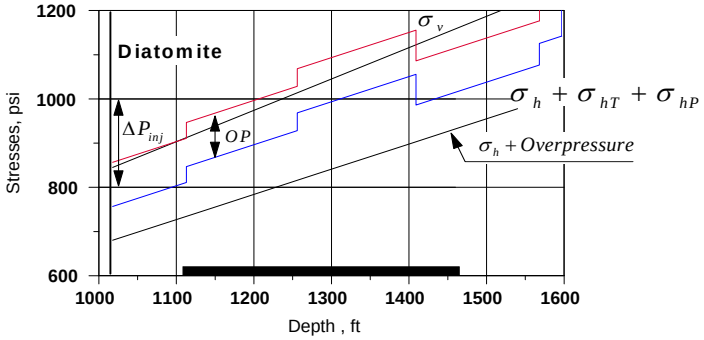

Fig. 21. - Thermal and pore pressure stresses resulting from heating and pressuring the rock around IN2U by 180^{0}F and 200 psi, respectively. Now only the horizontal fracture created earlier can